Eur. Phys. J. A (2022) 58:55
https://doi.org/10.1140/epja/s10050-022-00708-8

THE EUROPEAN PHYSICAL JOURNAL A

Regular Article - Theoretical Physics

Isoentropic equations of state of β-stable hadronic matter with a quark phase transition

Domenico Logoteta[1,2,a], **Ignazio Bombaci**[1,2], **Albino Perego**[3,4]

[1] Dipartimento di Fisica "Enrico Fermi", Università di Pisa, Largo B. Pontecorvo 3, 56127 Pisa, Italy
[2] INFN Sezione di Pisa, Largo B. Pontecorvo 3, 56127 Pisa, Italy
[3] Dipartimento di Fisica, Università di Trento, Via Sommarive 14, 38123 Trento, Italy
[4] INFN-TIFPA, Trento Institute for Fundamental Physics and Applications, via Sommarive 14, 38123 Trento, Italy

Received: 21 November 2021 / Accepted: 13 March 2022

Communicated by D.N. Voskresensky

Abstract We construct isoentropic equations of state (EOSs) of β-stable dense hadronic matter considering the possibility that a quark deconfinement phase transition can take place. These conditions can be actually realized in different astrophysical contexts like core-collapse supernovae (CCSNe), during the early stages of the evolution of a newly formed neutron star (protoneutron star, PNS) or in the postmerger compact object formed in binary neutron star (BNS) mergers. We consider four different EOSs to describe the hadronic phase: three EOSs from relativistic mean field theory and one EOS recently derived from microscopic calculations in the framework of the Brueckner–Hartree–Fock approach. We combine these hadronic EOSs with a quark matter EOS obtained from a modified MIT-Bag model which takes into account some perturbative corrections in the grand canonical potential due to the quark–quark interaction. The two phases are then joined up through a Gibbs construction. For each model we study thermal and neutrino trapping effects on the matter composition and consequently on the EOS. We finally determine the PNS static structure integrating the Tolman–Oppenheimer–Volkoff equations. We find that the thermal contribution and particularly the effect of neutrino trapping play an important role on the full EOS. The latter can get softer or stiffer according to the strangeness content in the hadronic phase. These effects are thus crucial to provide a proper description of the dynamical evolution of both the postmerger compact object formed in a BNS merger or the PNS formed in a CCSN.

1 Introduction

The physics of hot and dense matter is of interest for a large variety of different physical systems spanning from heavy-ion collisions to binary neutron star (BNS) mergers. The latter have received particular attention in the last years due to their strong connection with the physics of gravitational waves (GWs) and more in general of multimessenger astronomy [1–4]. The description of neutron stars (NSs) as well as of astrophysical events like core collapse supernovae (CCSNe) [5,6] and BNS mergers [7–9] requires the knowledge of the equation of state (EOS) of matter [10,11], namely the relation between pressure (P), energy density (ε) and temperature (T) for given matter composition. One of the greatest challenge here is the large variety of thermodynamic conditions that matter experiences in these events, spanning several orders of magnitude in all the relevant variables [11,12]. However, according to the specific system under investigation, matter can be characterized by definite thermodynamical conditions like low temperature or approximately constant entropy per baryon (S/A), at least over some timescales of interest. In particular in the present work we consider the specific situation in which S/A can be considered constant and we accordingly study and build up the corresponding EOS. The latter condition is expected to be realized in good approximation in the core of protoneutron stars (PNSs) [10,13–16] and in the compact object that forms after the merging of two neutron stars if a prompt collapse to a black hole (BH) does not take place [7,17–20]. Such a postmerger remnant can be possibly gravitational unstable and survive only a few milliseconds before collapsing into a BH, but it can also evolve into a long-lived massive NS, with a collapse timescale changing by orders of magnitudes or eventually evolve to a stable NS. The precise fate of the postmerger remnant and the collapse

[a] e-mail: domenico.logoteta@pi.infn.it (corresponding author)

Published online: 30 March 2022

timescale depend on several factors, including the masses and the spins of the colliding NSs, the properties of the EOS at supra-nuclear densities, the strength of the magnetic field and of all processes responsible for the redistribution of angular momentum inside the remnant. Indeed, several mechanisms can temporally prevent the collapse of the central object to a BH and the most relevant ones are the differential rotation of the remnant and the thermal support provided by dense matter in semi-degenerate conditions [7].

Another crucial point for the modeling of the above mentioned astrophysical phenomena is related to the composition of hot and dense matter. In fact due to the very large densities and/or temperatures reached in a PNS or in the postmerger remnant of a BNS merger, various hadronic species (in addition to nucleons) and phases of QCD matter are expected to appear. Hyperons are the first of such "exotic" constituents [21–25]. Moreover, a transition to a phase with deconfined quarks (quark matter) is also expected according to various QCD-inspired models [26–34]. The study of the quark deconfinement phase transition in hot and dense matter and of its implications for the structure and evolution of compact objects is one of the main objective of the present work.

Hot and dense matter in the center of CCSNe and BNS mergers produces copious quantities of neutrinos through weak interactions. Over the cooling timescale all neutrinos have escaped, the PNS or the long-lived BNS merger remnant has become transparent and cold and neutrino-less weak equilibrium (also called neutrino-less β-equilibrium) has been achieved. This is the case of cold, deleptonized NSs. However, during the early stages of the evolution of PNSs and BNS merger remnants, the neutrino diffusion time (~ 30 s) is larger than any relevant dynamical timescale and neutrinos can be considered as trapped (or partially trapped) and possibly in weak equilibrium with matter [7,10,13,15,35–37]). If this physical condition is actually realized for several seconds before neutrinos escape, the trapped neutrino component provides a contribution to the matter's pressure and alters the composition of the stellar material thus modifying the EOS with respect to the case of neutrino-free matter [10].

According to these considerations, it is relevant to ask if thermal and neutrino trapping effects act in direction to support the newly formed hot compact object against the collapse to BH or contrarily favor the collapse.

In the present work we thus study how these physical effects impact on the EOS of hot and dense matter, particularly how they influence the onset of the quark deconfinement phase transition, and as a whole how they affect the evolution of PNSs and BNS postmerger remnants. These effects may turn out to be important when encoded in numerical dynamical simulations of CCSNe and BNS mergers.

We want to emphasize that in the present work we assume that compact stars containing deconfined quarks are hybrid stars; in doing so we do not consider the possibility of the formation of the so called strange stars. The existence of the latter is based on the rightness of the hypothesis about the absolute stability of strange quark matter by Bodmer [38] and Witten [39], and it has been revised in light of the GW signal GW190814, whose light component was interpreted as a strange star of mass around $2.5 - 2.6\ M_{\odot}$ [40] (but see [41] or [42,43] for alternative interpretations).

The paper is organized as follows: in Sect. 2, we briefly review the EOSs adopted for both the hadronic and the quark matter phases. In the Sect. 3, we show results about the composition, temperature profiles and structure of hot compact remnants using isoentropic EOSs and considering various stellar conditions expected during the PNS evolution and/or dynamical astrophysical processes like BNS mergers and CCSNe. In the last section we outline the main conclusions of our work.

2 Equations of State

In our study we have considered four different EOS models to describe the hadronic phase (*i.e.* the phase of matter with quarks confined within baryons and mesons). In the first case the EOS is calculated making use of the non-relativistic Brueckner–Hartree–Fock (BHF) many-body approach, whereas the other three EOSs are constructed according to a relativistic mean field (RMF) model. The EOS for the quark phase, *i.e.* the phase of matter composed of the three lightest quark flavors, namely up (u), down (d) and strange (s) quarks, is modeled using an extended version of the MIT bag model.

For both the hadronic and the quark phases we consider matter in equilibrium, with respect to the weak interaction, with electrons (e^-), muons (μ^-), and eventually with neutrinos (in the case of matter with trapped neutrinos) and we include the contributions of all the corresponding antiparticles.

We next assume a first order phase transition between the two phases and, following Glendenning [44], we require global electric charge neutrality of bulk stellar matter. An important consequence of imposing global charge neutrality is that the hadronic and the quark phases can coexist over a finite range of pressures. This treatment of the phase transition is known in the literature as the Gibbs construction for the hadronic-quark mixed phase.

2.1 Hadronic matter EOS

In the first case the hadronic phase is modeled as a uniform fluid of neutrons and protons (nuclear matter) in β-equilibrium with electrons and muons, and possibly with neutrinos (in the case of matter with trapped neutrinos). The zero temperature version of this model (hereafter the

BL EOS) was derived in Ref. [45] within the BHF many-body approach making use of realistic two-nucleon (NN) [46] and three-nucleon (NNN) [47] interactions derived in in the framework of chiral effective field theory (χEFT) (e.g. [48,49]). These chiral nuclear interactions reproduce with high accuracy the nucleon-nucleon (NN) scattering data and the experimental binding energies of light (A = 3, 4) atomic nuclei. The BL EOS reproduces the empirical properties (energy per nucleon, symmetry energy and its slope parameter L, incompressibility) of nuclear matter at saturation density ($n_0 = 0.16\,\mathrm{fm}^{-3}$; see [47]), it does not violate causality (i.e. $v_s < c$, with v_s being the speed of sound in the nuclear medium), and it is consistent (see Fig. 2 in [45]) with the measured elliptic flow of matter in heavy-ion collisions experiments [50]. When computing static neutron star configurations, the BL EOS (for the β-stable case) gives a maximum mass $\mathrm{M_{max}} = 2.08\,\mathrm{M}_\odot$ (compatible with present measured NS masses [51–54]), and a quadrupolar tidal polarizability coefficient $\Lambda_{1.4} = 385$ (for the $1.4\,M_\odot$ neutron star [55]) compatible with the constraints derived from GW170817 [2,56]. Based on the universal relation derived in Ref. [20], the threshold mass for the prompt collapse to a BH for equal mass BNS mergers is $2.79\,M_\odot$ for this EOS, indicating that GW170817 is compatible with being a NS-NS system that did not undergo a prompt BH formation [18,20,57].

The BL EOS has been recently extended in Ref. [58] to finite temperature and out-of-β-equilibrium matter (hereafter the BLh EOS). This EOS model was successfully used in several numerical simulations of BNS mergers ([59–62]).

Moreover, the zero temperature version of this EOS was extended in Ref. [23] to include, in addition to neutrons and protons, the Λ hyperons. In particular, the authors of Ref. [23] have investigated the role of the three-baryon interaction ($NN\Lambda$) between two nucleon and a Λ hyperon on the EOS of hyperonic matter. It was found that it is possible to have hyperonic stars with a maximum mass of $\sim 2\,M_\odot$ when the NNΛ interaction is included in the Hamiltonian indicating a possible solution of the so called hyperon puzzle in neutron stars [63,64].

The second, the third and the forth hadronic EOSs we consider are based on a RMF scheme which includes nucleons: DD2 ([65]) and TM1-2 ([66]), or nucleons and hyperons: TM1-2Y ([66]). All the RMF models considered in this work are based on a quantum field theory Lagrangian density in which nucleons are assumed to interact via the exchange of effective σ, ω and ρ mesons. The equation of motion of the various fields are derived in the Hartree approximation. The TM1-2 model is a reparametrization of the original TM1 model ([67]) where the parameters entering in the Lagrangian density were adjusted (see Ref. [66]) in order to give, for the calculated pressure in symmetric nuclear matter, a result which is consistent with the measured elliptic flow of matter in collision experiments between heavy atomic nuclei [50]. Specifically, in the present work we use the parameters set denoted as TM1-2 in Table 1 of Ref. [68]. One of the main difference between the TM1-2 and the DD2 models is that the latter contains some density dependent terms in the Lagrangian density while the TM1-2 one has none. Both these two EOS models when used in NS structure calculations produce a quadrupolar tidal polarizability coefficient $\Lambda_{1.4}$ compatible with the constraints derived from GW170817 [1,56].

We remark that all the nucleonic EOS models used in our calculations, besides reproducing fairy well the empirical saturation density of nuclear matter $n_0 = 0.16 \pm 0.01\,\mathrm{fm}^{-3}$ and its corresponding energy per baryon $E/A_0 = -16.0 \pm 1.0$ MeV (e.g., [66]), predict values of the nuclear symmetry energy at saturation density in the interval $E_{\mathrm{sym}}(n_0) = 25 - 37$ MeV, and slope parameter $L = 30 - 90$ MeV, in agreement with several microscopic calculations as well as with experimental results [69,70]. The DD2 EOS model has been also widely employed in literature in numerical simulations of CCSNe [5,6] and BNS mergers [7,8]. Finally, the TM1-2Y is an extension of the TM1-2 model which includes the hyperons of the baryonic octect. The coupling constants that determine the interactions between nucleons and hyperons and between hyperons for this model were set in Ref. [68] using SU(6) symmetry and to reproduce reasonable values of the hyperons' single particle potentials at saturation density in symmetric nuclear matter. The maximum mass of NSs predicted by the TM1-2Y is compatible with measured NS masses having $M \sim 2\,M_\odot$.

At baryon density below $n \sim 0.05\,\mathrm{fm}^{-3}$ one has a transition to non-uniform nuclear matter. In this low density regime the DD2 and the TM1-2 models have a consistent extension up to very low density according to the very same RMF approach. For the BLh model this extension is not straightforward and it would require the solution of the Bethe-Goldstone equation in finite nuclei. In order to avoid this complication, we have instead used the procedure discussed in Ref. [58], namely for the low density part of the EOS we have smoothly matched the microscopic BHF calculations with the SFHo EOS [71].

2.2 Quark matter EOS

To model the quark phase we use an extended version of the phenomenological bag model EOS which includes the effects of gluon mediated QCD interactions between quarks up to the second order in the QCD coupling α_s [72–74]. The grand canonical potential per unit volume can be written as (we use units where $\hbar = c = 1$):

$$\Omega = \sum_f \Omega_f^0 + \frac{3}{4\pi^2}(1 - a_4)\mu^4 + B_{\mathrm{eff}} + \Omega_g^0 + \Omega_\gamma^0 \,. \qquad (1)$$

The first term on the right hand side of Eq. (1) gives the contributions to Ω originating from the fermionic constituents of matter, i.e. $f = u, d, s, e^-, \mu^-$ (and their antiparticles) with the possible addition of neutrinos and antineutrinos (in the case of matter with trapped neutrinos), all described as ideal relativistic Fermi gases. The second term on the right hand side of Eq. (1) accounts for the perturbative QCD corrections to $\mathcal{O}(\alpha_s^2)$ [72–74] and its value represents the degree of deviations from an ideal gas EOS, with $a_4 = 1$ corresponding to the ideal gas case. The chemical potential μ in Eq. (1) can be written in terms of the u, d and s quark chemical potentials as $\mu = (\mu_u + \mu_d + \mu_s)/3$. The term $B_{\rm eff}$ is an effective bag constant which takes into accounts in a phenomenological way nonperturbative aspects of QCD. We assume that both the a_4 and $B_{\rm eff}$ coefficient do not depend on the temperature. The last two terms in Eq. (1) represents the contributions from gluons and photons, both calculated as ideal Bose gases.

In the following we refer to this quark matter EOS model as effective MIT bag model (eMIT). We adopt two different parametrizations of this EOS that we refer to as: eMIT1 and eMIT2. In the first case we set: $B_{\rm eff} = 240$ MeV and $a_4 = 0.7$ while in the second: $B_{\rm eff} = 190$ MeV and $a_4 = 0.7$. These values have been chosen in such a way that, when the quark EOS is combined with a given hadronic EOS the maximum mass configuration of the resulting hybrid star sequence satisfies the two solar mass requirement [51–54].

2.3 EOS for protoneutron stars and postmerger remnants

We construct finite temperature and composition dependent NS EOSs by combining a hadronic and a quark EOS. We assume a smooth Gibbs construction [44] to join the hadronic and the quark phases. We thus require global electric charge neutrality of bulk stellar matter. As a consequence of this, the hadronic and the quark phases can coexist for a finite range of pressures. We are aware that, depending on the nature of the hadron-quark matter interface [75,76], other possibilities exist like to consider a sharp Maxwell construction [77] or to analyze the formation of specific matter geometries in the mixed phase (spheres, rods, ...) that minimize the total energy of the system, as discussed for instance in Ref. [78–80].

Moreover, in the case of matter with trapped neutrinos, we include electron and muon neutrinos (and their antiparticles) and describe them as as ideal relativistic Fermi gases in thermal and weak equilibrium with matter. In addition, we have fixed the value of the electronic lepton fraction to $Y_{L_e} = (n_e + n_{\nu_e})/n$ to $Y_{L_e} = 0.3$ and the muonic lepton fraction $Y_{L_\mu} = 0$, where n_e and n_{ν_e} are the net electron and electron neutrino densities, respectively. These values for Y_{L_i} are typical ones obtained in hydrodynamical simulations of the early stages of PNS. Throughout the paper we have kept these values of Y_{L_e} and Y_{L_μ} in the case of trapped neutrinos, unless explicitly specified. In the subsequent evolution, the cooling process is associated with a significant deleptonization towards cold neutrino-less weak equilibrium. It is important to stress that in the case of BNS mergers, matter is characterized by an initially low $Y_{L_e} \sim 0.1$, and experiences a leptonization process because of matter decompression and temperature increase. We emphasise that, in case of neutrino trapped matter, neutrinos have been included in the full EOS density range and not only in the high density regime.

We remark that we have included the contribution of the photons in all the density range of the EOSs considered in the present work. We additionally remark that even in the case of EOSs that take into account of a deconfinement phase transition, the assumption of constant entropy per baryon is kept. This last contest has been considered in a few works in the past [81–83]. A comment is in order: it is well known that during a first order phase transition the entropy per baryon is not constant but suffers a jump together with the total baryonic density of the system [84]. However, as pointed out in the previous works, stellar matter after phase transition can be considered again in a condition of approximately constant value of S/A. Such value will be different and in particular, due to neutrino diffusion, higher than the one before the phase transition. Clearly the precise value of the entropy variation should be calculated by a dynamical simulation while in the present work we can just address some general though qualitative behaviour.

Throughout the paper we adopt the following combinations of hadronic and quark EOS models: BLh+eMIT1, DD2+eMIT2, TM1-2+eMIT2 and TM1-2Y+eMIT2. Notice that when we combine the eMIT quark phase model to the DD2 and TM1-2 hadronic phase models various values of the ($B_{\rm eff}$, a_4) parameters can be adopted (in addition to the eMIT2 set) while keeping the two solar mass limit requirement for the resulting maximum mass hybrid star configuration. This is a consequence of the quite stiff behaviour of the EOS for these two models which allows for a large window of the quark matter parameters. The quark phase parameter space is instead strongly reduced in combination with the BLh model. This in turn reflects the softer character of the BLh model in comparison to the DD2 and TM1-2 ones. However for the analysis that we have carried out, the parameters choice is adequate to highlight the salient features of our discussion.

3 Results

In Fig. 1 we show the composition (i.e. the particle fractions Y_i for the various matter constituents) of β-stable stellar matter as a function of the baryon density n. In the left panel of this figure we present the particle fractions for the BLh+eMIT1 EOS for matter with constant entropy per baryon $S/A = 2$ in the case of neutrino-free matter (con-

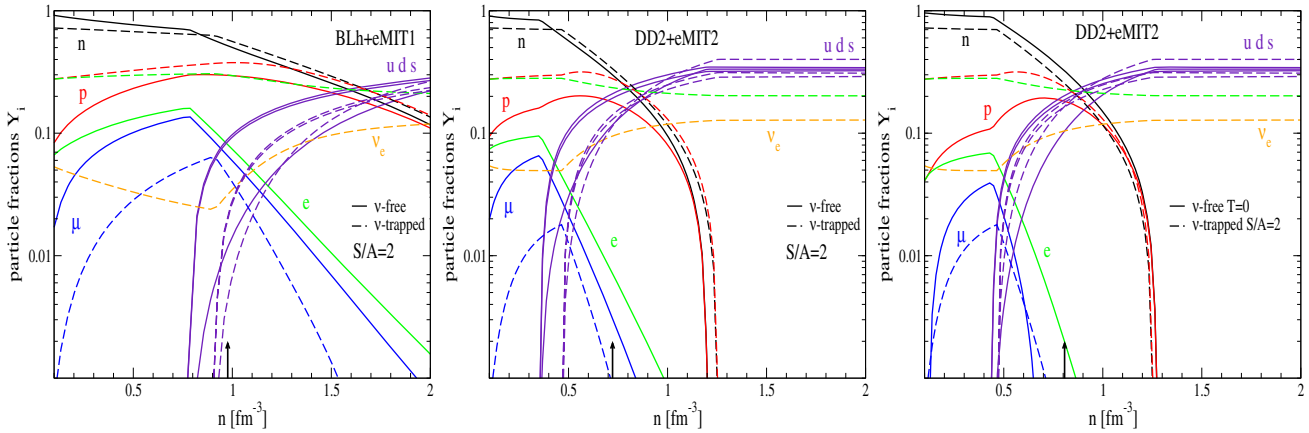

Fig. 1 Composition (i.e. particle fractions Y_i for the various matter constituents) of β-stable stellar matter as a function of the baryon density n. Left panel: particle fractions for the BLh+eMIT1 EOS for matter with constant entropy per baryon $S/A = 2$ in the case of neutrino-free matter (continuous lines) and neutrino-trapped matter with $Y_{L_e} = 0.3$ (dashed lines). Central panel: same as the left panel but for the DD2+eMIT2 EOS. Right panel: particle fractions for the DD2+eMIT2 EOS, in the case of cold ($T = 0$) neutrino-free matter (continuous lines) and $S/A = 2$ matter with trapped neutrinos (dashed lines). The upward pointing arrow in each panel denotes the central density of the stellar maximum mass configuration in the case of neutrino-free matter

tinuous lines) and neutrino-trapped matter with $Y_{L_e} = 0.3$ (dashed lines). As we can see neutrino trapping shifts the onset of the hadron-quark mixed phase to a larger density with respect to the neutrino-free matter case [10]. This behaviour can be explained as a consequence of the softening of the EOS of the pure nucleonic phase with trapped neutrinos compared to the neutrino-free case. In fact, in neutrino-trapped matter the chemical equilibrium conditions between nucleons, electrons and electron neutrinos reads:

$$\mu_n - \mu_p = \mu_e - \mu_{\nu_e}\,, \tag{2}$$

to be compared with $\mu_n - \mu_p = \mu_e$ in the case of neutrino free matter. Neutrino trapping, i.e. electronic and muonic lepton number conservation ($Y_{L_e} = 0.3$ and $Y_{L_\mu} = 0$ for the corresponding lepton fractions) during the early stages of PNS evolution produces an increase of the net electron fraction and consequently (due to charge neutrality) of the proton fraction (compare the corresponding dashed and continuous lines in Fig. 1 left panel) and makes nuclear matter more proton rich (i.e. more symmetric) and thus softer with respect to the neutrino-free case. The upward pointing arrow in each panel of Fig. 1 denotes the central density of the stellar maximum mass configuration in the case of ν-free matter. The corresponding arrow representing the same quantity for ν-trapped matter is very close (see 4th column in Table 1) to the one reported for the case of ν-free matter and it is not shown for clarity. The results reported in the left panel of Fig. 1 thus indicate that in the case of the BLh+eMIT1 EOS quark deconfinement occurs only in the core of stars with a mass close to the maximum mass configuration producing hybrid stars with a inner core with mixed hadron-quark phase. This outcome applies both to the case of neutrino free and neutrino trapped matter. Similar results are obtained for the composition of stellar matter in the case of the DD2+eMIT2 EOS model (Fig. 1 central panel). Again neutrino trapping shifts the onset of the mixed hadron-quark phase to a larger density compared to the neutrino free matter. Now quark deconfinement occurs at a lower density as compared to the previous case (BLh+eMIT1 EOS), but again the pure quark phase is not present in hybrid stars described by this EOS model. The different values for the onset of the mixed hadron-quark phase for the two models (BLh+eMIT1 and DD2+eMIT2) is essentially a consequence of the larger stiffness of the DD2 EOS with respect to the BLh EOS; this feature favours the onset of the phase transition at lower densities even assuming the same quark matter EOS for the two models.

In the right panel of Fig. 1, we compare the composition of matter with $S/A = 2$ and trapped neutrinos (dashed lines) with that of cold ($T = 0$) neutrino free matter (continuous lines) using the DD2+eMIT2 EOS model. These two cases represent the composition of matter in PNSs and in cold deleptonized NSs respectively. From the results in the right panel of Fig. 1, we see that the combined thermal ($S/A = 2$) and neutrino trapping effects shift the onset of the mixed phase to a slightly higher density with respect to the cold neutrino free case. To disentangle the outcome of the thermal effects on matter composition we can compare the results for $S/A = 2$ neutrino free matter (continuous lines in the central panel of Fig. 1) with those relative to $T = 0$ neutrino free matter (continuous lines in the right panel of Fig. 1). From this comparison we see that thermal effects move the threshold density for quark appearance to a lower value with respect to the $T = 0$ case. Thus thermal and neutrino trap-

ping effects have an opposite influence on the value of the baryon density where deconfined quarks appears in neutron star cores.

In Fig. 2 we show the temperature (T_S) of β-stable matter as a function of the baryon density along three different isoentropic paths ($S/A = 1,\ 2,\ 3$). Results in the left (middle) panel have been obtained using the BLh+eMIT1 (DD2+eMIT2) EOS model. The continuous (dashed) lines in both panels refer to the neutrino-free (neutrino trapped) matter case. For each curve in Fig. 2, T_S increases up to a maximum value which occurs for a value of the baryon density that is close to the one for the onset of the hadron-quark mixed phase.

The increase with baryon density of the temperature along isoentropic paths in the pure nucleonic phase can be explained using arguments grounded on the properties of mixtures of ideal degenerate Fermi gases [85–87]. For example for a degenerate mixture of non-interacting neutrons and protons, with densities n_n and n_p respectively, neutron-proton asymmetry $\beta = (n_n - n_p)/n = 1 - 2Y_p$ and neglecting the neutron-proton mass difference (m in Eq. (4) denotes the nucleon mass), the temperature of the system along isoentropic paths can be writen [85,86] as:

$$T_S = \chi(\beta)\ \frac{S}{A}\ n^{2/3}\,, \tag{3}$$

where

$$\chi(\beta) = \frac{\hbar^2}{m}\left(\frac{3}{\pi}\right)^{2/3}\left[\left(\frac{1+\beta}{2}\right)^{1/3} + \left(\frac{1-\beta}{2}\right)^{1/3}\right]^{-1}. \tag{4}$$

Thus for fixed entropy per nucleon and fixed density, T_S goes down by a factor $2^{-2/3} \sim 0.63$ going from pure neutron matter ($\beta = 1$) to symmetric nuclear matter ($\beta = 0$).

This argument can be extended to the case of degenerate ideal relativistic Fermi gases [87], as electrons, muons and neutrinos, coming into play in dense stellar matter. The same Fermi gas argument can be used to explain the decrease, at fixed baryon density, of T_S when neutrinos are trapped (dashed lines in Fig. 2) with respect to the case of neutrino-free matter (continuous lines in Fig. 2).

As the system enters in the mixed phase, T_S decreases (Fig. 2) with density. Again this behaviour can be understood using the argument based on the properties of mixtures of ideal degenerate Fermi gases and since the entropy is an extensive (i.e. additive) thermodynamic quantity. In fact, in the mixed phase one has the coexistence of nucleons (eventually hyperons), leptons and deconfined quarks and gluons. Thus the number of degrees of freedom in the mixed phase is larger than those in the pure hadronic (nucleonic) phase, accordingly for fixed S/A the temperature T_S of the system is lower than the corresponding one for the pure hadronic (nucleonic) phase at the same density. As the density of the mixed phase rises, the quark Fermi seas are increasingly populated whereas the nucleons, electrons and muons concentrations (see Fig. 1) go down. As a result T_S decreases with density in the mixed phase. Eventually, if stellar matter could enter in the pure quark phase, T_S will rise again with density (see central panel in Fig. 2).

As already pointed out in connection with the matter composition results (Fig. 1), hybrid star configurations computed using the BLh+eMIT1 and the DD2+eMIT2 EOS models have inner cores made of mixed hadron-quark matter. To illustrate this outcome we plot in the left and central panels of Fig. 2 a full circle on the top of each continuous line (neutrino-free matter) which represents the values of the central density and central temperature of the stellar maximum

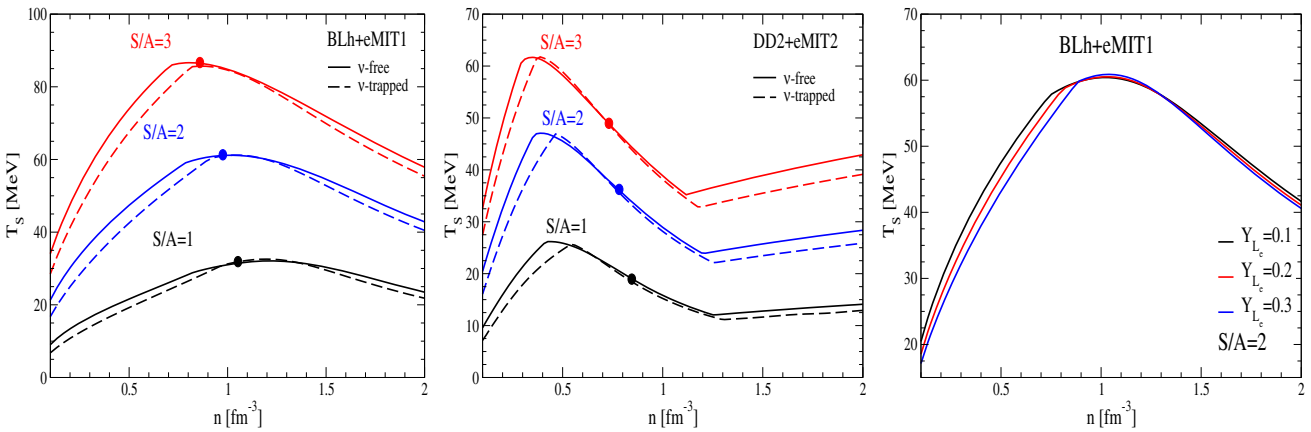

Fig. 2 Temperature profiles of β-stable EOSs for the BLh+eMIT1 model (left panel) and the DD2+eMIT2 model (middle panel) considering three values of S/A. Continuous (dashed) lines refer to the case of neutrino-free (-trapped) matter. In the right panel we show the variation of the temperature profiles according to three different values of Y_{L_e} and fixing $S/A = 2$. The heavy dots on the curves corresponding to the ν-free matter case denote the central density and temperature of the maximum neutron star mass configuration

mass configuration. Thus the portion of the $T_S(n)$ curve on the right of the full circle can not be realized in hybrid stars described by the EOS models used in Fig. 2. In the right panel of Fig. 2 we show the effect of the variation of the electronic lepton fraction Y_{L_e} on T_S (with $S/A = 2$) in the case of β-stable matter with trapped neutrinos using the BLh+eMIT1 EOS. Increasing the value of Y_{L_e} makes stellar matter more neutrino rich and again, for fixed values of S/A, lower temperatures are obtained. Results similar to those reported in Fig. 2 have been obtained in the case of the TM1-2+eMIT2 and TM1-2Y+eMIT2 EOS models.

In Fig. 3 we report the pressure as a function of the energy density for β-stable matter in the case of the BLh+eMIT1 EOS (left panel) and DD2+eMIT2 EOS (right panel) for three different values of the entropy per baryon ($S/A = 1, 2, 3$) in the case of neutrino-free matter (continuous lines) and matter with trapped neutinos (dashed lines). For both models the mixed hadron-quark phase is delimited by the two kinks in the pressure curves. The heavy dot in each of the continuous lines denotes the values of the central energy density and central pressure of the stellar maximum mass configuration in the case of ν-free matter. The largest outcome of thermal effects on the EOS is observed in the mixed hadron-quark phase. In this region the EOS becomes softer with increasing S/A both in the case of neutrino-free matter (continuous lines) and neutrino-trapped matter (dashed lines) [81]. This behaviour is opposite to what is obtained in the pure hadronic (nucleonic) phase, where thermal effects increase the pressure as the temperature or the entropy per baryon rises. We note however that in the latter case the effect of S/A on the EOS is small compared to that in the mixed phase and it can be barely be appreciated in Fig. 3. This reversal of the thermal effects in the mixed hadron-quark phase is mainly determined by the following two factors (see Fig. 3): (i) the onset of the mixed phase moves to smaller densities when S/A increases (as already noted analysing the results for matter's composition in Fig. 1); (ii) a larger values of S/A favour a larger quark fraction and, as a consequence, a smaller nucleonic content thus making the EOS of the mixed phase softer.

We now discuss the neutrino trapping effects on the EOS. Again the largest consequences of neutrino trapping on the EOS are observed in the mixed hadron-quark phase for all the considered values of S/A. As discussed in connection with the results reported in Fig. 1, neutrino trapping shifts the onset of the mixed phase to larger density with respect to the neutrino free matter case. As shown in Fig. 3 this density shift produces a significant net increase of the pressure in the mixed phase at fixed energy density [81]. In the pure hadronic phase the change of pressure due to neutrino trapping is small compared to the one in the mixed phase with neutrino trapping making the EOS stiffer (softer) at low (high) densities.

In the following lines we discuss the role of hyperons on the quark deconfinement phase transition and on the EOS of hot and dense stellar matter. We will pay special attention to the interplay between hyperon population and neutrino trapping to control the EOS of hybrid stars. For all the results reported in the following Figs. 4 and 5 the EOS for hadronic (hyperonic) phase has been derived using the TM1-2Y model whereas the EOS of the quark phase using the eMIT2 parametrization of the extended version of the MIT bag model.

In the left panel of Fig. 4 we show the composition of β-stable hyperonic matter with $S/A = 2$, in the case of neutrino free (continuous lines) and neutrino trapped (dashed lines) matter. As we can see neutrino trapping shifts the threshold densities for the various hyperon species to larger values [1] and makes the EOS of hyperonic matter stiffer (compare the dashed and continuous lines in the right panel of Fig. 4) in agreement with previous works (e.g. [10,88]. Again this outcome can be understood comparing the chemical equilibrium conditions in neutrino trapped and neutrino free matter.

In general the chemical potential μ_i of a baryon species i in β-stable matter with trapped neutrinos can be written as [10]:

$$\mu_i = b_i \mu_n - q_i (\mu_e - \mu_{\nu_e}) , \tag{5}$$

where b_i and q_i are the baryon number and the electric charge (in unit of the elementary electric charge) of the baryon species i, μ_n is the neutron chemical potential, and μ_e and μ_{ν_e} are the chemical potentials for electrons and electron neutrinos respectively. In the case of hyperonic matter using Eq. (5), the chemical potential for the Σ^- hyperon in neutrino trapped matter can be written as

$$\mu_{\Sigma^-} = \mu_n + (\mu_e - \mu_{\nu_e}) . \tag{6}$$

Since $(\mu_e - \mu_{\nu_e})$ in neutrino trapped matter is smaller than μ_e in neutrino free matter [10] and since μ_n decreases too, because matter becomes more proton rich (see Fig. 4 left panel), the right hand side of Eq. (6) decreases (at a given baryon density) when neutrinos are trapped. Thus the threshold density for the Σ^- hyperons is shifted to a larger density and their abundance decreases with respect to the neutrino free case (Fig. 4 left panel).

In the case of the Λ hyperon (or other charge neutral hyperons) the chemical equilibrium condition (5) gives $\mu_\Lambda = \mu_n$ both in neutrino free and neutrino trapped matter. At first glance it would seem that neutrino trapping has no effect on the condition of chemical equilibrium and therefore on the

[1] Looking at Fig. 4 (left panel), it seems that neutrino trapping moves the threshold densities for the Ξ^- and Ξ^0 hyperons to smaller densities with respect to the neutrino free case. However this is a misleading visual effect due to the value for minimum particle fraction $Y_{min} = 10^{-3}$ reported in the Y-axis of the figure. Using a smaller Y_{min} (e.g. 10^{-5}) makes clear that neutrino trapping shifts the threshold densities of the Ξ^- and Ξ^0 hyperons to larger values as for the case of the other hyperons of the bayon octet.

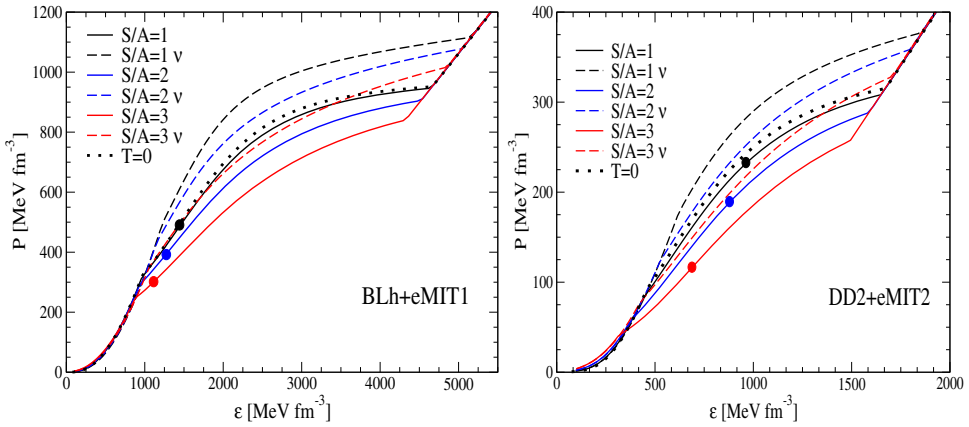

Fig. 3 Pressure P as a function of the energy density (ϵ) for β-stable matter in the case of the BLh+eMIT1 EOS (left panel) and DD2+eMIT2 EOS (right panel) for three different values of the entropy per baryon ($S/A = 1, 2, 3$) in the case of neutrino-free matter (continuous lines) and matter with trapped neutrinos (dashed lines). The heavy dot in each of the continuous lines denotes the values of the central energy density and central pressure of the stellar maximum mass configuration in the case of ν-free matter

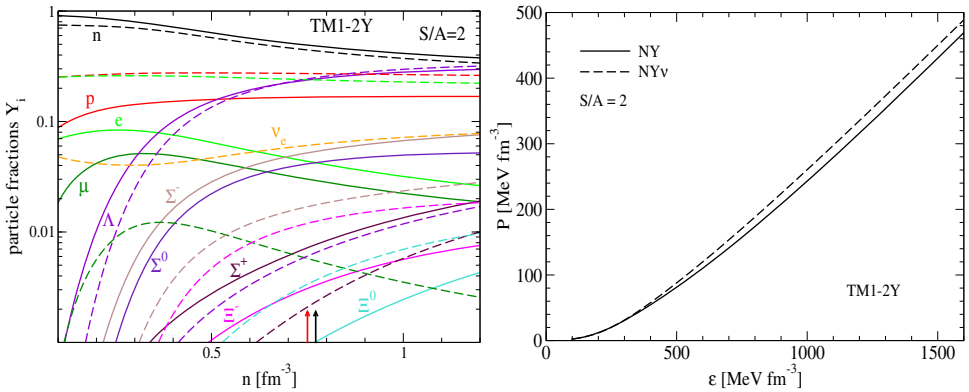

Fig. 4 Composition (left panel) and EOS (right panel) of β-stable hyperonic matter with constant entropy per baryon $S/A = 2$ in the case of neutrino free (continuous lines) and neutrino trapped matter with $Y_{L_e} = 0.3$ (dashed lines). The upward pointing black (red) arrow denotes the central density of the stellar maximum mass configuration in the case of neutrino free (neutrino trapped) matter. Results have been obtained using the TM1-2Y model

value of the threshold density for Λ hyperons. But obviously it is not so because the chemical potentials of neutrons and Λ hyperons change if we consider the case of trapped or untrapped neutrinos. In fact, as can be seen in Fig. 4 (left panel), neutrino trapping produces an increase of the proton fraction Y_p in β-stable nuclear matter and thus reduces the neutron fraction Y_n and the neutron chemical potential μ_n. Consequently neutrino trapping shifts the threshold density for the Λ hyperons to larger values in agreemment with the results reported the left panel of Fig. 4. As a result (Fig. 4 left panel) neutrino trapping produces a stiffening of the EOS of hyperonic matter [10,88].

We next discuss the interplay between neutrino trapping and the presence of hyperons on the threshold density for the mixed hadron-quark phase and on the EOS of hybrid star matter. First we consider the case with no hyperons and report in the left panel of Fig. 5 the composition of β-stable matter with $S/A = 2$ using the TM1-2+eMIT2 EOS. In accordance with the results obtained for the BLh+eMIT1 (Fig. 1 left panel) and the DD2+eMIT2 (Fig. 1 central panel) EOS models, again we find that neutrino trapping shifts the onset of the mixed hadron-quark phase to a larger density with respect to the neutrino free case. Afterwards we include hyperons among the constituents of the hadronic phase (NY matter) and use the TM1-2Y model to calculate its EOS. The composition of β-stable matter with $S/A = 2$ using the TM1-2Y+eMIT2 EOS is depicted in the right panel of Fig. 5. One more neutrino trapping shifts the onset of the hadron-quark mixed phase to a larger value compared to the neutrino free case.

To explore the role of hyperons on the quark deconfinement phase transition we compare the composition of β-

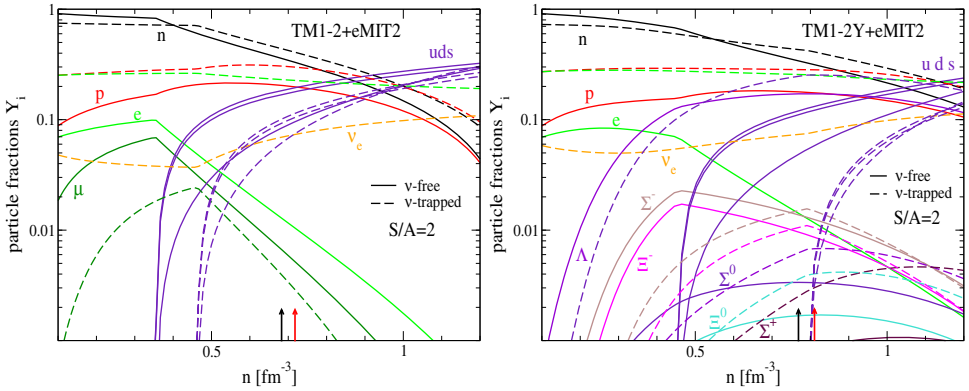

Fig. 5 Composition of β-stable hybrid star matter with constant entropy per baryon $S/A = 2$ as a function of the baryon density n in the case of neutrino free (continuous lines) and neutrino trapped (dashed lines) matter. Left panel: case with no hyperons using the TM1-2+eMIT2 EOS. Right panel: case with hyperons using the TM1-2Y+eMIT2 EOS. The upward pointing black (red) arrow, in both panels, denotes the central density of the stellar maximum mass configuration in the case of neutrino free (neutrino trapped) matter

stable stellar matter without and with hyperons depicted respectively in the left and right panels of Fig. 5. This comparison reveals that the presence of hyperons moves the threshold density for the hadron-quark mixed phase to a higher value with respect to the case where hyperons are not present [10]. This is true both in the case of neutrino free matter (continuous lines in the left and right panel in Fig. 5) and in the case of neutrino trapped matter (dashed lines in the left and central panel in Fig. 5).

The neutron star structure is determined by integrating the Tolman–Oppenheimer–Volkoff (TOV) equations which describe the hydrostatic equilibrium in general relativity for a spherical non-rotating body [26,27]. The calculated gravitational maximum mass ($M_{G,max}$), baryonic maximum mass ($M_{B,max}$), and the corresponding stellar radius (R) and central baryon density (n_c for the various EOS models used in this work are reported in Tab. 1.

The gravitational mass as a function of the radius (hereafter the mass-radius relation) is shown in the left and central panel of Fig. 6 for the BLh+eMIT1 and DD2+eMIT2 models respectively for different thermodynamic situations. First of all, it is interesting to note a different behaviour of the two EOS models concerning the dependence on the entropy per baryon of the gravitational maximum mass. In the case of the BLh+eMIT1 EOS model $M_{G,max}$ is almost constant with increasing S/A whereas in the case of the DD2+eMIT2 $M_{G,max}$ decreases with S/A. For example in the case of the DD2+eMIT2 model and neutrino free-matter $M_{G,max}$ decreases of about 5% passing from $T = 0$ to $S/A = 2$. As we already pointed out discussing the results in the left panel of Fig. 1, in the case of the BLh+eMIT1 EOS quark deconfinement occurs only in the core of stars with a mass close to the maximum mass configuration producing hybrid stars with a small inner core with mixed hadron-quark phase. Thus for this EOS model deconfined quarks does not have a sizeable influence on the maximum mass. Consequently the present results for $M_{G,max}(S/A)$ are in line with the finding of Ref. [10,89] for nucleonic stars and accordingly the maximum mass does not change significantly as function of of S/A. We want to remark that adopting the BLh model for the confined phase and employing a different parametrization of the quark matter EOS that allows to obtain a larger quark content in the final hybrid star configurations, a behaviour similar of the DD2+eMIT2 model is recovered. However such alternative parametrizations (like the eMIT2 one for instance) do not allow to satisfy the two solar mass limit and have been therefore ruled out.

In the right panel of Fig. 6 we report the mass-radius relations for the TM1-2 and TM1-2Y models, at fixed entropy per baryon $S/A = 2$, considering different possible matter compositions as described in details in the figure caption. Concerning the cases in which only nucleonic degrees of freedom are considered the behaviours are very similar to the corresponding ones for the DD2 model. It is interesting to note instead that when hyperons are included in the system, together with a trapped neutrino component, the maximum mass supported is larger than the corresponding one for hyperonic neutrino free matter. This is clearly in agreement with the scenario discussed in Fig. 3. This shows that according to the different composition of hot neutron star matter and in particular to the strangeness content, neutrinos can act in such a way to stabilize the system against collapse to BH like in the case of hyperonic matter, or go in the opposite direction like in the case of nucleonic matter.

The early evolution of a PNS is driven by thermal and neutrino trapping effects on the EOS. The main features of this process can be schematically investigated considering the following two snapshots of the evolution process:

Table 1 Maximum mass configuration properties for the various EOS models and thermodynamic conditions (first column) used in this work

EOS model	$M_{\mathrm{G,max}}$ $[M_\odot]$	R [km]	n_c [fm^{-3}]	$M_{\mathrm{B,max}}$ $[M_\odot]$
BLh $T = 0$	2.070	10.18	1.175	2.457
BLh $S/A = 1$	2.076	10.37	1.141	2.446
BLh $S/A = 2$	2.082	10.81	1.098	2.390
BLh $S/A = 3$	2.088	11.97	0.992	2.296
BLh $S/A = 1\ \nu$	2.021	10.39	1.190	2.323
BLh $S/A = 2\ \nu$	2.034	10.92	1.129	2.289
BLh $S/A = 3\ \nu$	2.051	12.07	1.018	2.223
BLh+eMIT1 $S/A = 1$	2.015	11.04	1.053	2.353
BLh+eMIT1 $S/A = 2$	2.017	11.74	0.982	2.296
BLh+eMIT1 $S/A = 3$	2.031	13.59	0.851	2.217
BLh+eMIT1 $S/A = 1\ \nu$	2.004	10.74	1.163	2.299
BLh+eMIT1 $S/A = 2\ \nu$	2.014	11.49	1.049	2.259
BLh+eMIT1 $S/A = 3\ \nu$	2.030	12.80	0.959	2.195
BLh+eMIT1 $T = 0$	2.015	10.60	1.253	2.374
DD2 $T = 0$	2.422	11.90	0.839	2.923
DD2 $S/A = 1$	2.417	12.02	0.844	2.889
DD2 $S/A = 2$	2.424	12.72	0.790	2.822
DD2 $S/A = 3$	2.448	13.95	0.735	2.747
DD2 $S/A = 1\ \nu$	2.385	12.38	0.834	2.776
DD2 $S/A = 2\ \nu$	2.396	12.97	0.771	2.729
DD2 $S/A = 3\ \nu$	2.424	14.20	0.737	2.676
DD2+eMIT2 $S/A = 1$	2.131	12.80	0.761	2.474
DD2+eMIT2 $S/A = 2$	2.050	13.78	0.725	2.299
DD2+eMIT2 $S/A = 3$	1.980	16.64	0.575	2.128
DD2+eMIT2 $S/A = 1\ \nu$	2.288	13.17	0.786	2.634
DD2+eMIT2 $S/A = 2\ \nu$	2.252	14.12	0.726	2.525
DD2+eMIT2 $S/A = 3\ \nu$	2.214	16.25	0.619	2.392
DD2+eMIT2 $T = 0$	2.159	12.52	0.809	2.536
TM1-2 $T = 0$	2.256	12.14	0.862	2.660
TM1-2 $S/A = 2$	2.296	13.49	0.773	2.639
TM1-2 $S/A = 2\ \nu$	2.265	14.87	0.763	2.546
TM1-2+eMIT2 $S/A = 2$	2.001	14.52	0.686	2.236
TM1-2+eMIT2 $S/A = 2\ \nu$	2.192	15.81	0.720	2.442
TM1-2Y $T = 0$	1.98	12.15	0.880	2.291
TM1-2Y $S/A = 2$	1.992	13.41	0.838	2.236
TM1-2Y $S/A = 2\ \nu$	2.079	15.27	0.803	2.300
TM1-2Y+eMIT2 $S/A = 2$	1.936	13.93	0.771	2.161
TM1-2Y+eMIT2 $S/A = 2\ \nu$	2.080	15.03	0.802	2.300
TM1-2Y+eMIT2 $T = 0$	1.956	12.28	0.861	2.257

Gravitational maximum mass M_G (second column), stellar radius R (third column), central baryon density n_c (forth column), baryonic maximum mass (M_B). EOS models for neutrino-trapped matter are denoted with the extra label ν in the first column

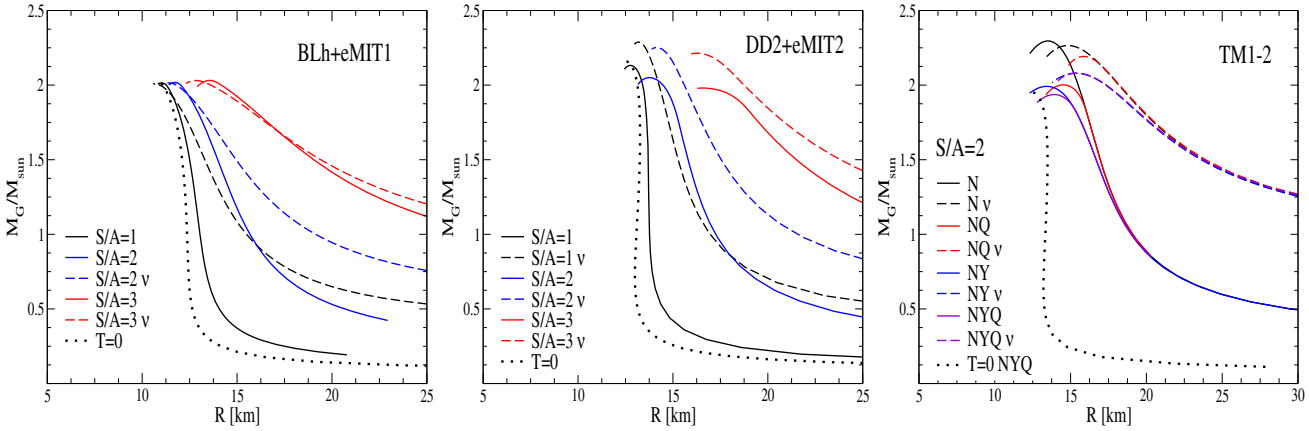

Fig. 6 Mass-radius relation for isoentropic stars. The first two panels illustrate the dependence of the mass-radius curve on the value of the entropy per baryon S/A and the effect of neutrino trapping (dashed lines) in the case of the BLh+eMIT1 model (left panel) and the DD2+eMIT2 model (central panel). In the right panel we show the mass-radius relation, for the TM1-2 and TM1-2Y models, considering different possible matter compositions: pure nucleonic matter (curves labeled N), nucleons plus hyperons (curves labeled NY), nucleons plus quark matter (curves labeled NQ), nucleons plus hyperons plus quark matter (curves labeled NYQ). For each of these matter's compositions we consider both the neutrino-free matter case and the neutrino-trapped case (curves with the extra label ν). In all three panels we also include the mass-radius curve for cold ($T = 0$) stars (dotted lines)

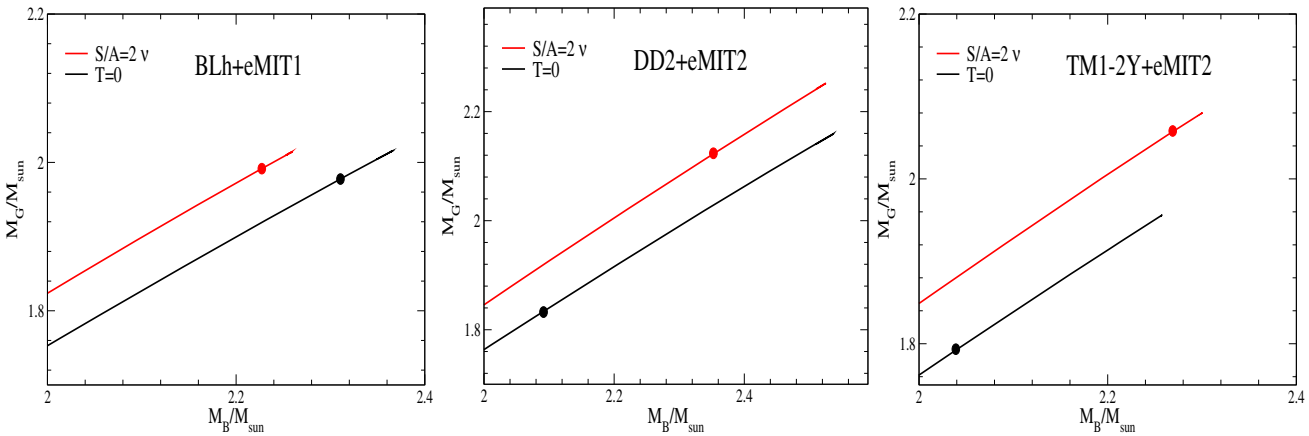

Fig. 7 Gravitational mass as function of the baryonic mass for the BLh+eMIT1 model (left panel), the DD2+eMIT2 model (central panel) and the TM1-2 model (right panel). In each panel the red upper curves refer to β-stable matter with $S/A = 2$ and trapped neutrinos while black curves describe the cold deleptonized neutron stars. In the right panel the red dotted (red continuous) line represents stellar configurations which include (do not include) the presence of hyperons in hot matter. In each curve the terminal point represents the maximum mass configuration, whereas the circles on each curve denote the the stellar configuration with central density equal to the onset of the mixed hadron-quark phase for the specific stellar conditions considered

(i) the hot PNS at a time $t \sim 3$ s after core bounce ($t = 0$), described by the isoentropic EOS with trapped neutrinos;
(ii) the cold and deleptonized NS at $t \sim 30$ s (neutrino diffusion time), described by the cold and neutrino-free EOS.

Since most of the matter accretion on the forming NS happens in the very early stages after birth ($t < 3$ s) [90], the neutron star baryonic mass M_B [91] stays almost constant during the evolution between these two configurations. Thus the evolution of a PNS can be unambiguously analyzed in the M_G–M_B plane [92] (see also [82]). To this purpose we show in Fig. 7 the gravitational mass as a function of the baryonic mass for the following stellar sequences: (i) PNSs (red lines), i.e. isoentropic EOS with $S/A = 2$ and trapped neutrinos with $Y_{l_e} = 0.3$, (ii) cold deleptonized NSs (black lines), with $T = 0$ and neutrino-free matter, in the case of the BLh+eMIT1 (left panel), DD2+eMIT2 (central panel), and TM1-2Y+eMIT2 (right panel) EOS models. The end point on each curve represents the corresponding maximum mass configuration, which we denote as $M^{(i)}_{\mathrm{G\,max}}$ and $M^{(i)}_{\mathrm{B\,max}}$ for the PNS sequence, and with $M^{(f)}_{\mathrm{G\,max}}$ and $M^{(f)}_{\mathrm{B\,max}}$ for the final

cold deleptonized NS sequence. The values of these quantities, for the considered EOS models, are reported in Tab. 1. The circle, on each curve in Fig. 7, represents the stellar configuration with a central density equal to the onset of the mixed hadron-quark phase for the considered EOS model and stellar conditions. Thus all neutron star configurations with a baryonic mass larger than the one corresponding to the circle contains a mixed phase core (hybrid stars). We denote the baryonic masses of the stellar configurations associated to these circles as $M^{(i)}_{B,q}$ (red circle) and $M^{(f)}_{B,q}$ (black circle) with similar notation for the corresponding stellar gravitational masses.

To begin with we consider the BLh+eMIT1 EOS model (Fig. 7, left panel). A PNS born with a baryonic mass $M^{(i)}_B < M^{(i)}_{B,q}$ does not contain quark matter (nucleonic PNS). This star will evolve to the cold deleptonized nucleonic star having a gravitational mass $M^{(f)}_G$ and the same baryonic mass of the initial PNS configuration i.e. $M^{(f)}_B = M^{(i)}_B$. The total binding energy of the star will increase by $\Delta B = (M^{(i)}_G - M^{(f)}_G)c^2$. This energy will be released mainly through neutrino emission. PNSs born with a baryonic mass in the range $M^{(i)}_{B,q} < M^{(i)}_B \leq M^{(i)}_{B,max}$ are hot hybrid stars. As shown by our results in Fig. 7 (left panel), these stars will evolve to cold deleptonized nucleonic stars. In other words, in this stellar baryonic mass range neutrino escape and stellar cooling trigger a reconfinement phase transition (i.e. a transition from deconfined quark matter to nucleonic matter) in the stellar core. This peculiar behaviour of the evolution of PNSs, in the above quoted baryonic mass range, can be interpreted comparing the values of the central pressure in the PNS and in the final cold deleptonized NS. For example, considering $M^{(i)}_B = 2.241\, M_\odot$ the central pressure of the star goes down from 452 MeV/fm^3 (PNS) to 232 MeV/fm^3 (NS). At this "low" value of the pressure in cold neutrino free matter, the quark phase has a larger Gibbs energy per nucleon with respect to that of the nucleonic phase, thus a transition to the nucleonic phase take place [93]. We next consider a PNS with $M^{(i)}_{\rm B\,max} < M^{(i)}_{\rm B} \leq M^{(f)}_{\rm B\,max}$. In this case the PNS can not be supported by the matter pressure against gravitational collapse since its baryonic mass $M^{(i)}_{\rm B}$ is greater than the maximum possible baryonic mass $M^{(i)}_{\rm B\,max}$ for the initial configuration. Thus the collapsing stellar core will collapse to a BH after reaching supranuclear densities. In the classical analysis *à la* Oppenheimer–Volkoff, where the dynamical evolution of the PNS is not taken into account, stars in this baryonic mass range will be considered to have a stable equilibrium configuration in the cold deleptonized stellar sequence. Thus the gravitational mass $M^*_{\rm G\,max} \equiv M^{(f)}_{\rm G}(M^{(i)}_{\rm B\,max})$ of the star corresponding to the evolution of the maximum mass PNS configuration, plays the role of an *effective maximum mass* for the cold deleptonized NS sequence [92]. Finally when $M^{(i)}_{\rm B} > M^{(f)}_{\rm B\,max}$ the stellar core will collapse to a BH.

Consider now a NS in a binary stellar system in which the companion star is a normal star. If during the evolution of the binary system a common envelope is formed the NS can accrete matter from its companion star with a certain accretion rate $\dot{M}_{\rm B}$. After a sufficiently long time the NS could increase its baryonic mass above the value $M^{(i)}_{\rm B\,max}$ and it will start to populate the portion of the final NS sequence with $M^{(i)}_{\rm B\,max} < M_{\rm B} \leq M^{(f)}_{\rm B\,max}$, eventually reaching and then overcoming the Oppenheimer–Volkoff maximum mass configuration $M^{(f)}_{\rm B\,max}$. Thus, as pointed out for the first time in [92], in the baryonic mass range $[M^{(i)}_{\rm B\,max}, M^{(f)}_{\rm B\,max}]$ one can have both NSs and BHs. In the case of the BLh+eMIT1 EOS model (Fig. 7, left panel) this matter accretion mechanism is the only way to form hybrid stars, since PNS evolution will always produces nucleonic stars.

A similar analisys can be done in the case of the DD2+eMIT2 EOS model (Fig. 7, central panel). In particular, in the baryonic mass range $[M^{(f)}_{\rm B\,q}, M^{(i)}_{\rm B\,q}]$ the quark deconfinement phase transition will take place during the evolution of the newly born star, and a pure nucleonic PNS will evolve to a cold deleptonized hybrid star.

The evolution of PNSs described by TM1-2Y+eMIT2 EOS model (Fig. 7, right panel) shares many common features with those described by the DD2+eMIT2 model, with one major exception: in the case TM1-2Y+eMIT2 EOS model, PNSs with a baryonic mass in the range $[M^{(f)}_{\rm B\,max}, M^{(i)}_{\rm B\,max}]$ after neutrino escape and cooling will collapse to black holes. This outcome is related to the presence of hyperons among the stellar constituents in the TM1-2Y model and to role played by neutrino trapping on the EOS. In fact, neutrino trapping (as discussed in the previous pages) shifts the onset of hyperons (and of the quark deconfinement phase transition) to larger density values with respect to those for neutrino free matter, making as a consequence the EOS of PNS matter stiffer and thus resulting in $M^{(i)}_{\rm B\,max} > M^{(f)}_{\rm B\,max}$.

4 Discussion and conclusions

In this work, we have carried out a study of hot β-stable neutrino trapped and neutrino free hadronic matter EOS considering the possibility that a quark deconfinement phase transition can take place. In this study we have considered the case in which the entropy per baryon, S/A, can be analyzed as constant since this condition is expected to be realized in the inner core of neutron stars during some stages of the evolution of high energy astrophysical phenomena like CCSNe or BNSs mergers. We have employed four different EOSs to describe the hadronic phase, namely the BLh, DD2, TM1-2 and TM1-2Y. We have then combined these hadronic EOSs

with a quark matter EOS derived from a modified MIT-Bag model which takes into account some perturbative corrections in the grand-canonical potential due to the quark-quark interaction. We have finally performed a Gibbs construction to join up the two phases.

We have found that according to the strangeness content in the hadronic phase, the thermal contribution and the effect of neutrino trapping can get the EOS softer or stiffer. In particular the presence of hyperonic degrees of freedom in neutrino trapped matter produces a stiffer EOS compared to the case of neutrino free matter. In addition, the neutrino trapped component moves the onset of the phase transition to higher densities. The central density corresponding to the maximum mass configuration can accordingly lay in the mixed phase or in the quark phase. For the parametrizations adopted in the present work none of our models shows the formation of a pure quark phase in the final star configurations. Note however that a pure quark phase could be efficiently realized in dynamical BNS merger simulations [94–97]. Another very important point is that the metastable object that can be formed after the merging of two neutron stars is at least initially in a state of differential rotation. A more realistic description would indeed require the integration of the equations for differentially rotating neutron stars using stellar conditions similar to the ones that we have discussed in this paper. Differentially rotating neutron stars [98–101] represent indeed the previous stage to the one described in this paper and in some sense trigger the existence of the final star configurations obtained in the present work. These issues will be the topic of a forthcoming work.

Based on our results, we conclude that the effects described in the present paper are crucial for dynamical simulations of BNSMs and CCSNe and may affect the stability of the compact object formed after the neutron star-neutron star merging process.

Data Availability Statement This manuscript has no associated data or the data will not be deposited. [Authors' comment: Data are available upon reasonable request to the corresponding author.]

References

1. B.P. Abbott et al., Phys. Rev. Lett. **119**(16), 161101 (2017). https://doi.org/10.1103/PhysRevLett.119.161101
2. B.P. Abbott et al., Phys. Rev. Lett. **121**, 161101 (2018). https://doi.org/10.1103/PhysRevLett.121.161101
3. B.P. Abbott et al., Astrophys. J. Lett. **892**(1), L3 (2020). https://doi.org/10.3847/2041-8213/ab75f5
4. R. Abbott et al., Astrophys. J. Lett. **896**(2), L44 (2020). https://doi.org/10.3847/2041-8213/ab960f
5. A. Burrows, Rev. Mod. Phys. **85**, 245 (2013). https://doi.org/10.1103/RevModPhys.85.245
6. H.T. Janka, T. Melson, A. Summa, Annu. Rev. Nucl. Part. Sci. **66**(1), 341 (2016). https://doi.org/10.1146/annurev-nucl-102115-044747
7. D. Radice, S. Bernuzzi, A. Perego, Ann. Rev. Nucl. Part. Sci. **70**, 95 (2020). https://doi.org/10.1146/annurev-nucl-013120-114541
8. M. Shibata, K. Hotokezaka, Ann. Rev. Nucl. Part. Sci. **69**, 41 (2019). https://doi.org/10.1146/annurev-nucl-101918-023625
9. L. Baiotti, L. Rezzolla, Rep. Prog. Phys. **80**(9), 096901 (2017). https://doi.org/10.1088/1361-6633/aa67bb
10. M. Prakash, I. Bombaci, M. Prakash, P.J. Ellis, J.M. Lattimer, R. Knorren, Physics Reports **280**(1), 1 (1997) 10.1016/S0370-1573(96)00023-3. https://www.sciencedirect.com/science/article/pii/S0370157396000233
11. M. Oertel, M. Hempel, T. Klähn, S. Typel, Rev. Mod. Phys. **89**(1), 015007 (2017). https://doi.org/10.1103/RevModPhys.89.015007
12. A. Perego, S. Bernuzzi, D. Radice, Eur. Phys. J. A **55**(8), 124 (2019). https://doi.org/10.1140/epja/i2019-12810-7
13. A. Burrows, J.M. Lattimer, ApJ **307**, 178 (1986). https://doi.org/10.1086/164405
14. W. Keil, H.T. Janka, Astron. Astrophys. **296**, 145 (1995)
15. J.A. Pons, S. Reddy, M. Prakash, J.M. Lattimer, J.A. Miralles, ApJ **513**(2), 780 (1999). https://doi.org/10.1086/306889
16. G. Camelio, A. Lovato, L. Gualtieri, O. Benhar, J.A. Pons, V. Ferrari, Phys. Rev. D **96**(4), 043015 (2017). https://doi.org/10.1103/PhysRevD.96.043015
17. K. Hotokezaka, K. Kyutoku, H. Okawa, M. Shibata, K. Kiuchi, Phys. Rev. D **83**, 124008 (2011). https://doi.org/10.1103/PhysRevD.83.124008
18. A. Bauswein, T.W. Baumgarte, H.T. Janka, Phys. Rev. Lett. **111**(13), 131101 (2013). https://doi.org/10.1103/PhysRevLett.111.131101
19. F. Zappa, S. Bernuzzi, D. Radice, A. Perego, T. Dietrich, Phys. Rev. Lett. **120**(11), 111101 (2018). https://doi.org/10.1103/PhysRevLett.120.111101
20. S. Köppel, L. Bovard, L. Rezzolla, Astrophys. J. Lett. **872**(1), L16 (2019). https://doi.org/10.3847/2041-8213/ab0210
21. N.K. Glendenning, ApJ **293**, 470 (1985). https://doi.org/10.1086/163253
22. D. Chatterjee, I. Vidaña, Eur. Phys. J. A **52**(2), 29 (2016). https://doi.org/10.1140/epja/i2016-16029-x
23. D. Logoteta, I. Vidaña, I. Bombaci, Eur. Phys. J. A **55**(11), 207 (2019). https://doi.org/10.1140/epja/i2019-12909-9
24. A. Sedrakian, A. Harutyunyan, Universe **7**(10), 382 (2021). https://doi.org/10.3390/universe7100382
25. D. Logoteta, Universe **7**(11), 408 (2021). https://doi.org/10.3390/universe7110408
26. N.K. Glendenning, *Compact stars: Nuclear physics, particle physics, and general relativity* (1997)
27. J. Schaffner-Bielich, *Compact Star Physics* (Cambridge University Press, 2020). https://doi.org/10.1017/9781316848357
28. J.D. Walecka, *Theoretical nuclear and subnuclear physics*, vol. 16 (1995)

29. P. Braun-Munzinger, J. Wambach, Rev. Mod. Phys. **81**(3), 1031 (2009). https://doi.org/10.1103/RevModPhys.81.1031
30. I. Bombaci, D. Logoteta, I. Vidaña, C. Providência, Eur. Phys. J. A **52**(3), 58 (2016). https://doi.org/10.1140/epja/i2016-16058-5
31. A. Drago, A. Lavagno, G. Pagliara, D. Pigato, Eur. Phys. J. A **52**(2), 40 (2016). https://doi.org/10.1140/epja/i2016-16040-3
32. D. Alvarez-Castillo, A. Ayriyan, S. Benic, D. Blaschke, H. Grigorian, S. Typel, Eur. Phys. J. A **52**(3), 69 (2016). https://doi.org/10.1140/epja/i2016-16069-2
33. S. Benic, D. Blaschke, D.E. Alvarez-Castillo, T. Fischer, S. Typel, Astron. Astrophys. **577**, A40 (2015). https://doi.org/10.1051/0004-6361/201425318
34. I. Bombaci, D. Logoteta, Mon. Not. R. Astron. Soc. **433**, L79 (2013). https://doi.org/10.1093/mnrasl/slt064
35. T. Fischer, S.C. Whitehouse, A. Mezzacappa, F.K. Thielemann, M. Liebendorfer, Astron. Astrophys. **517**, A80 (2010). https://doi.org/10.1051/0004-6361/200913106
36. L. Hüdepohl, B. Müller, H.T. Janka, A. Marek, G.G. Raffelt, Phys. Rev. Lett. **104**, 251101 (2010). https://doi.org/10.1103/PhysRevLett.104.251101
37. L.F. Roberts, G. Shen, V. Cirigliano, J.A. Pons, S. Reddy, S.E. Woosley, Phys. Rev. Lett. **108**, 061103 (2012). https://doi.org/10.1103/PhysRevLett.108.061103
38. A.R. Bodmer, Phys. Rev. D **4**, 1601 (1971). https://doi.org/10.1103/PhysRevD.4.1601
39. E. Witten, Phys. Rev. D **30**, 272 (1984). https://doi.org/10.1103/PhysRevD.30.272
40. I. Bombaci, A. Drago, D. Logoteta, G. Pagliara, I. Vidaña, Phys. Rev. Lett. **126**, 162702 (2021). https://doi.org/10.1103/PhysRevLett.126.162702
41. A. Gupta, D. Gerosa, K.G. Arun, E. Berti, W.M. Farr, B.S. Sathyaprakash, Phys. Rev. D **101**, 103036 (2020). https://doi.org/10.1103/PhysRevD.101.103036
42. E.R. Most, L.J. Papenfort, L.R. Weih, L. Rezzolla, Mon. Not. R. Astron. Soc. **499**(1), L82 (2020). https://doi.org/10.1093/mnrasl/slaa168
43. V. Dexheimer, R.O. Gomes, T. Klähn, S. Han, M. Salinas, Phys. Rev. C **103**, 025808 (2021). https://doi.org/10.1103/PhysRevC.103.025808
44. N.K. Glendenning, Phys. Rev. D **46**, 1274 (1992). https://doi.org/10.1103/PhysRevD.46.1274
45. I. Bombaci, D. Logoteta, Astron. Astrophys. **609**, A128 (2018). https://doi.org/10.1051/0004-6361/201731604
46. M. Piarulli, L. Girlanda, R. Schiavilla, K. A., A. Lovato, L.E. Marcucci, S.C. Pieper, M. Viviani, R.B. Wiringa, Phys. Rev. C **94**, 054007 (2016). https://doi.org/10.1103/PhysRevC.94.054007
47. D. Logoteta, I. Bombaci, A. Kievsky, Phys. Rev. C **94**, 064001 (2016). https://doi.org/10.1103/PhysRevC.94.064001
48. R. Machleidt, D.R. Entem, Phys. Rep. **503**(1), 1 (2011). https://doi.org/10.1016/j.physrep.2011.02.001
49. H.W. Hammer, S. König, U. van Kolck, Rev. Mod. Phys. **92**(2), 025004 (2020). https://doi.org/10.1103/RevModPhys.92.025004
50. P. Danielewicz, R. Lacey, W.G. Lynch, Science **298**, 1592 (2002). https://doi.org/10.1126/science.1078070
51. P. Demorest, T. Pennucci, S. Ransom, M. Roberts, J. Hessels, Nature **467**, 1081 (2010). https://doi.org/10.1038/nature09466
52. J. Antoniadis, P.C.C. Freire, N. Wex, T.M. Tauris, R.S. Lynch, M.H. van Kerkwijk, M. Kramer, C. Bassa, V.S. Dhillon, T. Driebe, J.W.T. Hessels, V.M. Kaspi, V.I. Kondratiev, N. Langer, T.R. Marsh, M.A. McLaughlin, T.T. Pennucci, S.M. Ransom, I.H. Stairs, J. van Leeuwen, J.P.W. Verbiest, D.G. Whelan, Science **340**(6131), 448 (2013). https://doi.org/10.1126/science.1233232
53. H.T. Cromartie et al., Nat. Astron. **4**(1), 72 (2019). https://doi.org/10.1038/s41550-019-0880-2
54. E. Fonseca et al., Astrophys. J. Lett. **915**(1), L12 (2021). https://doi.org/10.3847/2041-8213/ac03b8
55. D. Logoteta, I. Bombaci, Universe **5**(10), 204 (2019). https://doi.org/10.3390/universe5100204
56. B.P. Abbott et al., Phys. Rev. X **9**(3), 031040 (2019). https://doi.org/10.1103/PhysRevX.9.031040
57. A. Bauswein, S. Blacker, V. Vijayan, N. Stergioulas, K. Chatziioannou, J.A. Clark, N.U.F. Bastian, D.B. Blaschke, M. Cierniak, T. Fischer, Phys. Rev. Lett. **125**(14), 141103 (2020). https://doi.org/10.1103/PhysRevLett.125.141103
58. D. Logoteta, A. Perego, I. Bombaci, Astron. Astrophys. **646**, A55 (2021). https://doi.org/10.1051/0004-6361/202039457
59. A. Endrizzi, D. Logoteta, B. Giacomazzo, I. Bombaci, W. Kastaun, R. Ciolfi, Phys. Rev. D **98**(4), 043015 (2018). https://doi.org/10.1103/PhysRevD.98.043015
60. S. Bernuzzi et al., Mon. Not. R. Astron. Soc. **497**(2), 1488 (2020). https://doi.org/10.1093/mnras/staa1860
61. V. Nedora, S. Bernuzzi, D. Radice, B. Daszuta, A. Endrizzi, A. Perego, A. Prakash, M. Safarzadeh, F. Schianchi, D. Logoteta, Astrophys. J. **906**(2), 98 (2021). https://doi.org/10.3847/1538-4357/abc9be
62. V. Nedora, D. Radice, S. Bernuzzi, A. Perego, B. Daszuta, A. Endrizzi, A. Prakash, F. Schianchi, Mon. Not. R. Astron. Soc. **506**(4), 5908 (2021). https://doi.org/10.1093/mnras/stab2004
63. I. Bombaci, J.P.S. Conf, Proc. **17**(101002), 8 (2017). https://doi.org/10.7566/JPSCP.17.101002
64. I. Bombaci, Nucl. Phys. News **31**(3), 17 (2021). https://doi.org/10.1080/10619127.2021.1915024
65. S. Typel, G. Röpke, T. Klähn, D. Blaschke, H.H. Wolter, Phys. Rev. C **81**, 015803 (2010). https://doi.org/10.1103/PhysRevC.81.015803
66. D. Logoteta, C. Providência, I. Vidaña, Phys. Rev. C **88**, 055802 (2013). https://doi.org/10.1103/PhysRevC.88.055802
67. Y. Sugahara, H. Toki, Prog. Theor. Phys. **92**, 803 (1994). https://doi.org/10.1143/PTP.92.803
68. C. Providencia, A. Rabhi, Phys. Rev. C **87**(5), 055801 (2013). https://doi.org/10.1103/PhysRevC.87.055801
69. B.A. Li, B.J. Cai, W.J. Xie, N.B. Zhang, Universe **7**(6), 182 (2021). https://doi.org/10.3390/universe7060182
70. B.A. Li, X. Han, Phys. Lett. B **727**, 276 (2013). https://doi.org/10.1016/j.physletb.2013.10.006
71. A.W. Steiner, M. Hempel, T. Fischer, ApJ **774**(1), 17 (2013). https://doi.org/10.1088/0004-637X/774/1/17
72. E.S. Fraga, A. Kurkela, A. Vuorinen, Astrophys. J. Lett. **781**(2), L25 (2014). https://doi.org/10.1088/2041-8205/781/2/L25
73. M. Alford, M. Braby, M. Paris, S. Reddy, Astrophys. J. **629**, 969 (2005). https://doi.org/10.1086/430902
74. S. Weissenborn, I. Sagert, G. Pagliara, M. Hempel, J. Schaffner-Bielich, Astrophys. J. Lett. **740**, L14 (2011). https://doi.org/10.1088/2041-8205/740/1/L14
75. G. Lugones, Eur. Phys. J. A **52**(3) (2016). https://doi.org/10.1140/epja/i2016-16053-x
76. G. Lugones, A.G. Grunfeld, Universe **7**(12) (2021). https://doi.org/10.3390/universe7120493
77. A. Bhattacharyya, I.N. Mishustin, W. Greiner, J. Phys. G **37**, 025201 (2010). https://doi.org/10.1088/0954-3899/37/2/025201
78. G. Watanabe, T. Maruyama, K. Sato, K. Yasuoka, T. Ebisuzaki, Phys. Rev. Lett. **94**(3) (2005). https://doi.org/10.1103/PhysRevLett.94.031101
79. N. Yasutake, T. Maruyama, T. Tatsumi, J. Phys. Conf. Ser. **312**(4), 042027 (2011). https://doi.org/10.1088/1742-6596/312/4/042027
80. K. Maslov, N. Yasutake, D. Blaschke, A. Ayriyan, H. Grigorian, T. Maruyama, T. Tatsumi, D.N. Voskresensky, Phys. Rev. C **100**(2) (2019). https://doi.org/10.1103/PhysRevC.100.025802
81. A. Steiner, M. Prakash, J.M. Lattimer, Phys. Lett. B **486**, 239 (2000). https://doi.org/10.1016/S0370-2693(00)00780-2

82. M. Mariani, M. Orsaria, H. Vucetich, Astron. Astrophys. **601**, A21 (2017). https://doi.org/10.1051/0004-6361/201629315
83. H. Chen, G.F. Burgio, H.J. Schulze, N. Yasutake, Astron. Astrophys. **551**, A13 (2013). https://doi.org/10.1051/0004-6361/201220718
84. I. Bombaci, D. Logoteta, P.K. Panda, C. Providencia, I. Vidaña, Phys. Lett. B **680**, 448 (2009). https://doi.org/10.1016/j.physletb.2009.09.039
85. I. Bombaci, T.T.S. Kuo, U. Lombardo, Phys. Lett. B **311**(1–4), 9 (1993). https://doi.org/10.1016/0370-2693(93)90524-L
86. I. Bombaci, T.T.S. Kuo, U. Lombardo, Phys. Rep. **242**(1–3), 165 (1994). https://doi.org/10.1016/0370-1573(94)90149-X
87. A.W. Steiner, M. Prakash, J.M. Lattimer, Phys. Lett. B **486**(3–4), 239 (2000). https://doi.org/10.1016/S0370-2693(00)00780-2
88. I. Vidana, I. Bombaci, A. Polls, A. Ramos, Astron. Astrophys. **399**, 687 (2003). https://doi.org/10.1051/0004-6361:20021840
89. I. Bombaci, M. Prakash, M. Prakash, P.J. Ellis, J.M. Lattimer, G.E. Brown, Nucl. Phys. A **583**, 623 (1995). https://doi.org/10.1016/0375-9474(94)00736-7
90. R.A. Chevalier, ApJ **346**, 847 (1989). https://doi.org/10.1086/168066
91. I. Bombaci, B. Datta, Astrophys. J. Lett. **530**, L69 (2000). https://doi.org/10.1086/312497
92. I. Bombaci, Astron. Astrophys. **305**, 871 (1996)
93. I. Bombaci, D. Logoteta, C. Providencia, I. Vidaña, Astron. Astrophys. **528**, A71 (2011). https://doi.org/10.1051/0004-6361/201015783
94. E.R. Most, L.J. Papenfort, V. Dexheimer, M. Hanauske, S. Schramm, H. Stöcker, L. Rezzolla, Phys. Rev. Lett. **122**, 061101 (2019). https://doi.org/10.1103/PhysRevLett.122.061101
95. A. Bauswein, N.U.F. Bastian, D.B. Blaschke, K. Chatziioannou, J.A. Clark, T. Fischer, M. Oertel, Phys. Rev. Lett. **122**, 061102 (2019). https://doi.org/10.1103/PhysRevLett.122.061102
96. L.R. Weih, M. Hanauske, L. Rezzolla, Phys. Rev. Lett. **124**, 171103 (2020). https://doi.org/10.1103/PhysRevLett.124.171103
97. A. Prakash, D. Radice, D. Logoteta, A. Perego, V. Nedora, I. Bombaci, R. Kashyap, S. Bernuzzi, A. Endrizzi, Phys. Rev. D **104**(8), 083029 (2021). https://doi.org/10.1103/PhysRevD.104.083029
98. T.W. Baumgarte, S.L. Shapiro, M. Shibata, Astrophys. J. **528**(1), L29 (2000). https://doi.org/10.1086/312425
99. F. Galeazzi, S. Yoshida, Y. Eriguchi, Astron. Astrophys. **541**, A156 (2012). https://doi.org/10.1051/0004-6361/201016316
100. J.D. Kaplan, C.D. Ott, E.P. O'Connor, K. Kiuchi, L. Roberts, M. Duez, Astrophys. J. **790**, 19 (2014). https://doi.org/10.1088/0004-637X/790/1/19
101. D. Gondek-Rosinska, I. Kowalska, L. Villain, M. Ansorg, M. Kucaba, Astrophys. J. **837**(1), 58 (2017). https://doi.org/10.3847/1538-4357/aa56c1